

pubs.acs.org/JACS Article

# Amalgamation of DNAzymes and Nanozymes in a Coronazyme

Li Zuo, Kehao Ren, Xianming Guo, Pravin Pokhrel, Bishal Pokhrel, Mohammad Akter Hossain, Zhao-Xu Chen, Hanbin Mao,\* and Hao Shen\*



Cite This: J. Am. Chem. Soc. 2023, 145, 5750-5758



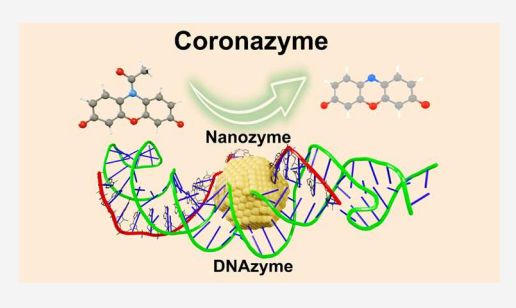
**ACCESS** 

Metrics & More

Article Recommendations

Supporting Information

ABSTRACT: Artificial enzymes such as nanozymes and DNAzymes are economical and stable alternatives to natural enzymes. By coating Au nanoparticles (AuNPs) with a DNA corona (AuNP@DNA), we amalgamated nanozymes and DNAzymes into a new artificial enzyme with catalytic efficiency 5 times higher than AuNP nanozymes, 10 times higher than other nanozymes, and significantly greater than most of the DNAzymes on the same oxidation reaction. The AuNP@DNA demonstrates excellent specificity as its reactivity on a reduction reaction does not change with respect to pristine AuNP. Single-molecule fluorescence and force spectroscopies and density functional theory (DFT) simulations indicate a long-range oxidation reaction initiated by radical production on the AuNP surface,



followed by radical transport to the DNA corona, where the binding and turnover of substrates take place. The AuNP@DNA is named coronazyme because of its natural enzyme mimicking capability through the well-orchestrated structures and synergetic functions. By incorporating different nanocores and corona materials beyond DNAs, we anticipate that the coronazymes represent generic enzyme mimics to carry out versatile reactions in harsh environments.

#### INTRODUCTION

Enzymes are natural catalysts with exceptional reactivity and substrate selectivity. However, their applications are limited since enzymes suffer from insufficient stability under operating conditions, narrow substrate scope, and high costs. Over the past decade, artificial enzymes such as  $nanozymes^{1-5}$  and  $DNAzymes^{6-10}$  have been developed to overcome the limitations of natural enzymes. While nanozymes usually comprise stable and affordable metals or metal oxides as core materials, DNAzymes employ versatile and programmable DNA fragments as essential components to catalyze enzymatic reactions. Chimera enzymes have been assembled using the structures of nanozymes and DNAzymes. 11,12 However, these chimera assemblies only demonstrate incremental improvement in catalytic functions without synergistically integrating the core activities of respective artificial enzymes. Recently biomolecules, e.g., DNA, have been coated on nanozymes to enhance biocompatibility and control substrate accessibility, 11,13,14 but they do not directly participate in catalytic

In contrast, catalytic reactions are carried out by DNA templates in DNAzymes, which are most promising among all biomaterials because of their fully programmable structure and versatile interactions with many ligands, 8,9,11 including metals. Similar to the well-known protein corona, the decoration of DNA on nanoparticles readily forms a DNA corona. The noncatalytic roles of the DNA corona 24,25 during nanozyme catalysis remain unclear since controversial observations exist among DNA-based biohybrid nanozymes: some studies suggest that DNAs inhibit the catalytic activities of parent

nanoparticles because of their hindrance to surface sites<sup>26,27</sup> while others suggest that DNAs could enhance catalytic reactivity by facilitating substrate adsorption.<sup>28,29</sup>

In this work, we discovered that a DNA corona decorating a 5 nm AuNP directly catalyzes an oxidation reaction per se (Figure 1a and Supporting Information Section S3), an unprecedented phenomenon that breaks the boundary between DNAzymes and nanozymes. Despite being the most stable element on the periodic table, gold surprisingly mimics a wide range of natural enzymes such as oxidase, peroxidase, catalase, and nuclease. Consequently, AuNPs were most intensively investigated as a nanozyme material. Here, a DNA hairpin consisting of two poly(adenosine) internal loops in its stem was prepared, which could strongly bind to AuNPs to form the DNA corona. To avoid the ubiquitous heterogeneity in single particles, single-molecule spectroscopy<sup>30</sup> was used to probe fluorogenic reactions occurring on the AuNP@DNA. We detailed the reaction mechanism by dissecting the two components, the DNA corona and AuNP nanocore, using single-molecule kinetics. Due to the presence of the DNA corona, the AuNP@DNA exhibited better catalytic reactivity ( $k_{cat}n$ , n is the number of reaction sites) and superior reaction selectivity  $(K_{M'}$  the Michaelis constant)

Received: November 21, 2022 Published: February 16, 2023





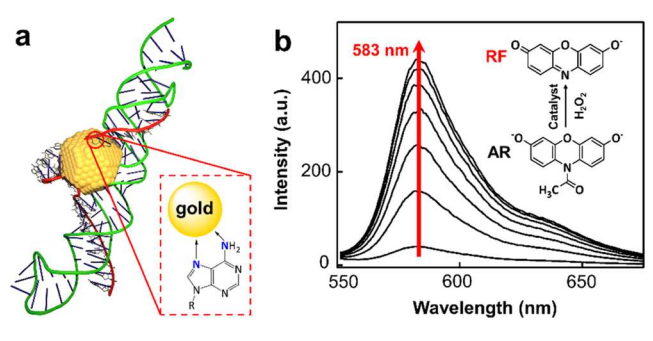




Figure 1. Single-molecule fluorogenic reaction on the AuNP@DNA coronazyme. (a) Schematic of the AuNP@DNA. A DNA hairpin binds to a 5 nm Au nanosphere through the two poly(adenosine) strands in the internal loop of its stem (see Supporting Information 3.1 for details). (b) N-Deacetylation of AR generates a fluorescent product resorufin (RF, emission ~ 583 nm), in a 50 mM pH 7.4 sodium phosphate buffer. (c) Scheme of the single-molecule reactivity measurement. Nanozymes are immobilized on the surface with reactants constantly flowing over. A 532 nm laser is configured in total internal reflection geometry to excite RFs generated on the nanozymes. An ultrasensitive sCMOS camera captures the emission signals.

compared to pristine 5 nm AuNPs or other nanozymes. Furthermore, its efficiency  $(k_{\rm cat}n/K_{\rm M})$  is higher than most of the DNAzymes working on the same amplex red (AR) substrate. Using DFT calculations and single-molecule force spectroscopy, we revealed the role and function of the DNA corona during coronazyme catalysis. Our results indicate that an enzyme mimicking reactivity is initiated at the nanocore of the AuNP@DNA while carried out remotely within the DNA corona, hence the name coronazyme. Such a remote catalysis mechanism is widely applicable for more efficient designs of artificial enzymes by separately optimizing structures and functions of the nanocores and corona phases.

## **■ EXPERIMENTAL SECTION**

Synthesis of Poly(A)-Functionalized AuNPs. The sequences of oligonucleotides are listed in Supporting Information Table S1. The synthesis of a poly(A)-DNA template contained three major steps (Supporting Information Section S3): (1) the synthesis of oligonucleotides (ppd1.1-ppd1.5); (2) pairing up ppd1.2-ppd1.3 and ppd1.4-ppd1.5; and (3) ligation among ppd1.1, annealed ppd1.2-ppd1.3, and annealed ppd1.4-ppd1.5.

The citrate-capped Au colloidal solution was mixed with poly(A)-DNA in the 1:10 mole ratio. The mixture was kept at  $-80\,^{\circ}\mathrm{C}$  for  $\sim 15\,$  min, during which a ligand exchange process occurred by replacing citrate with adenine of the DNA. The mixture was then rapidly thawed at room temperature to redistribute particles in the solution. Ultraviolet—visible (UV—vis) spectra and transmission electron microscopy (TEM) images of the as-prepared sample are shown in Supporting Information Figures S2 and S3. The surface-bound DNA corona prevents aggregation and well suspends the AuNP@DNA in solution

**Ensemble Catalytic Reactions.** Two fluorogenic reactions were used in this work to determine the catalytic performances of nanozymes. They are (1) the N-deacetylation of AR oxidation by  $H_2O_2$  to generate the high-fluorescence product resorufin (RF), acetate, and water; and (2) the N-deoxygenation of resazurin (RZ) reduction by  $NH_2OH$  to generate RF and nitrite. Ensemble catalysis was carried out to confirm the effective catalytic conversions on AuNPs by measuring the fluorescence spectra and absorption of RF (Supporting Information Section S4).

Single-Molecule Fluorescence Microscopy and Data Analyses. Detailed procedures of single-molecule catalysis and data analyses are provided in Supporting Information Sections S6 and S7. Briefly, nanozymes were immobilized within a homemade microfluidic chamber, which was assembled between a microscope slide and a piece of coverslip. This chamber was connected to a syringe pump for the continuous supply of reaction mixture (20  $\mu$ L/min) and placed under a TIR fluorescence microscope during the reaction (Supporting Information Figure S10). Then, 0.1–1.8  $\mu$ M AR and 60

mM H<sub>2</sub>O<sub>2</sub> were dispersed in 50 mM pH 7.4 phosphate buffer for the AR oxidation reaction, while 0.05-0.6 µM RZ and 1 mM NH<sub>2</sub>OH were dispersed in 50 mM pH 7.4 phosphate buffer for the RZ reduction reaction. A 532 nm continuous wave laser beam (DragonLaser) of  $\sim$ 8 mW was focused onto an area of  $\sim$ 35  $\times$  35 um<sup>2</sup> to excite the fluorescence of the product RF. The fluorescence emission signals were collected using a 100× N.A. 1.49 oil immersion objective (UAPON 100xOTIRF, Olympus) and filtered using a longpass (Chroma, ET542lp) and a bandpass (Chroma ET575/50 m) filter. The resulting signals were captured with an sCMOS camera (Photometrics Prime 95B) through Olympus CellSens Dimension software at a frame rate of 33 fps. The images were then analyzed using ThunderSTORM, 31,32 an ImageJ plugin program, in combination with a home-written Matlab program to localize the positions of individual fluorescent product molecules (Supporting Information Section S7.1 and Figure S11). AuNPs (40 nm) were visible because of their photoluminescence signals (Supporting Information Figure S14B), therefore an additional background subtraction step was taken before further analysis.

Single-Molecule Mechanochemical Experiments and Data Analysis. The DNA-AuNP and DNA-reaction substrate interactions were investigated in a dual-trap laser-tweezer instrument,<sup>33</sup> as described in Supporting Information Section S5. The laser-tweezer setup (Supporting Information Figure S8) contained a ligated 1558 bp dsDNA handle to the left and a 2391 bp dsDNA handle to the right of the synthesized DNA hairpin. To evaluate the interaction between poly(A)-DNA and AuNPs, the AuNP@DNA construct was tethered between the two beads after bringing the DNA-conjugated streptavidin-coated polystyrene bead close to the antidig antibodycoated bead. To evaluate the interaction between poly(A)-DNA and reaction substrates, the DNA construct was first tethered as described above, and then, AR, RZ, or RF with desired concentrations was supplied to the chamber. Tension on the DNA construct was developed when the two optically trapped beads were moved apart by steering one of the trapping lasers. Upon moving two beads apart, the tethered DNA was stretched. The tension produced on the DNA-AuNP/substrate conjugate was calculated based on the spring constant of each trap and the displacement of the bead from the center of the trap. The FX curves were recorded through a LabView program (National Instruments, Austin, TX) at 1 kHz with a loading rate of 5.5 pN/s (in the 10-30 pN force range), and data treatment was performed using Matlab (The MathWorks) and Igor (Wave-Metrics) programs.

Theoretical Calculations. The interactions between DNA and substrate molecules were investigated using DFT calculations. Calculation procedures are detailed in Supporting Information Section S10. Briefly, all of the calculations were performed with the Gaussian16 package at the B3LYP-D3BJ/6-31++G\*\* level. Frequency calculations were performed at the same theoretical level to guarantee that all of the structures obtained were local minima (no

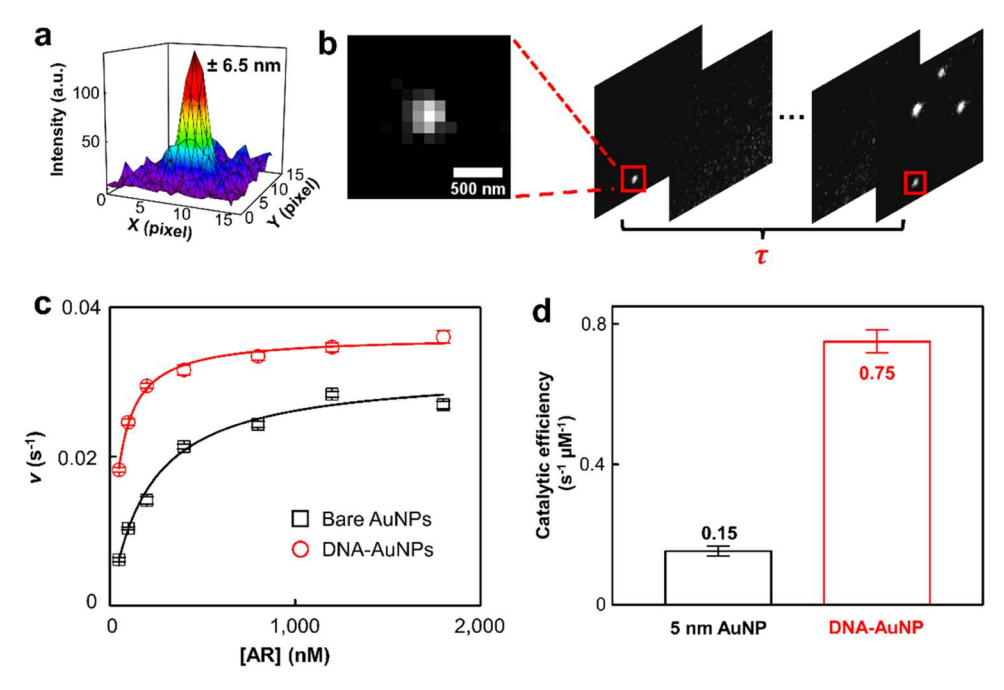


Figure 2. Single-molecule AR oxidation. (a) Localizing an RF molecule by fitting its emission signal to a two-dimensional Gaussian function. The localization error is 6.5 nm. (b) Extraction of reaction waiting time  $\tau$  for a single catalyst. Nanozymes are identified by grouping the RFs in consecutive frames using the nearest-neighbor method. The dark time before the generation of a fresh RF is the waiting time  $\tau$  for a single turnover. (c) Dependence of the single-catalyst turnover rate  $\nu$  on the AR concentration for the nanozyme-catalyzed reaction.  $[H_2O_2] = 60$  mM. The error bars depict standard errors of the mean. Each data point is an average of more than 80 nanozymes. (d) Comparison of the catalytic efficiency for the 5 nm AuNP against the AuNP@DNA.

imaginary frequencies) on the potential energy surfaces. An SMD model described the solvation effects with the dielectric constant  $\varepsilon=2.4$ . The visual illustration of the interactions between the substrate and the bases was produced with the method of an independent gradient model based on Hirshfeld partition (IGMH) implemented in the Multiwfn 3.8 program package.

## RESULTS AND DISCUSSION

Single-Molecule Peroxidase Kinetics of AuNP@DNA **Coronazymes.** AuNPs are a peroxidase mimic. Hence, we used AR, a well-known fluorogenic substrate for peroxidase, to determine its catalytic performances (Figure 1b, inset, and Supporting Information Section S4.1). In the presence of H<sub>2</sub>O<sub>2</sub> and a 5 nm AuNP, the nonfluorescent AR readily converts to a highly fluorescent molecule RF with its emission at ~583 nm (Figure 1b). Single-molecule catalysis was carried out inside a microfluidic chamber, in which nanozymes were pre-immobilized (Figure 1c and Supporting Information Section S6). The formation of the reaction product RF in a 50 mM sodium phosphate buffer (pH 7.4) at 25 °C was seen as reoccurring fluorescence bursts at the same location because RF was only generated on the surface of the nanozyme one at a time. There were multiple nanozymes in the  $\sim$ 35  $\times$  35  $\mu$ m<sup>2</sup> field of view, so superlocalization imaging was performed to ensure the correct assignment of RF molecules to their parent nanozymes. Briefly, the centroids of each emission spot within a frame were fitted to two-dimensional Gaussians to achieve tens of nanometer resolution (Figure 2a). The nearestneighbor searching was performed across consecutive frames to assign centroids of RF to different nanozymes (Supporting Information Section S7.1). The waiting time,  $\tau$ , between two consecutive RF formations from the same nanozyme depicts a single-reaction turnover time (Figure 2b). The statistical values

of many  $\tau$  on the same nanozyme reflect the catalytic properties of the nanozyme.

The average turnover rate  $\langle \tau \rangle^{-1}$  ( $\langle \cdot \rangle$  denotes averaging) at the 5 nm AuNP increases with increasing AR concentration until its saturation point (Figure 2c, black). The [AR]-dependent reactivity well matches with modified Michaelis—Menten kinetics

$$\langle \tau \rangle^{-1} = k_{\text{cat}} n[S] / (K_{\text{M}} + [S]) \tag{1}$$

In which  $k_{\text{cat}}$  is the rate constant for a single reactive site, n is the number of reactive sites within one nanozyme,  $K_{\rm M}$  is the Michaelis-Menten constant, and [S] is the substrate concentration (Supporting Information Section S7.5). For the 5 nm AuNP,  $k_{\rm cat}n$  and  $K_{\rm M}$  are 0.031  $\pm$  0.001 s<sup>-1</sup> and 0.21  $\pm$ 0.02  $\mu$ M, respectively. The catalytic efficiency  $k_{\rm cat}n/K_{\rm M}$  equals 0.15  $\pm$  0.01 s<sup>-1</sup>  $\mu$ M<sup>-1</sup>, lower than that of natural peroxidase HRP<sup>34</sup> (~2.84 s<sup>-1</sup>  $\mu$ M<sup>-1</sup>). Surprisingly, adding the DNA corona to the AuNP significantly enhanced the peroxidase reactivity (Figure 2c, red; see Supporting Information and ref 23 for detailed preparation). The saturation reactivity for the AuNP@DNA is higher than that of the original 5 nm AuNP. By fitting the curve with eq 1, it is found that the  $k_{cat}n$  and  $K_{M}$ are  $0.0360 \pm 0.0003 \text{ s}^{-1}$  and  $0.048 \pm 0.002 \mu\text{M}$ , respectively. A significant decrease of  $K_{\rm M}$  indicates that the AR interacts with the AuNP@DNA much stronger than the 5 nm AuNP. Moreover, the AuNP@DNA exhibited the similar activity heterogeneity as its parent 5 nm AuNP<sup>35</sup> (Supporting Information Section \$7.6). Overall, the catalytic efficiency  $(k_{\rm cat}n/K_{\rm M})$  has a 5 times increase to 0.75  $\pm$  0.03 s<sup>-1</sup>  $\mu$ M<sup>-1</sup>, suggesting that the AuNP@DNA is a much more efficient catalyst than its parent AuNP (Figure 2d). To the best of our knowledge, this is one of the highest catalytic efficiencies among all of the reported nanozymes for AR oxidation.

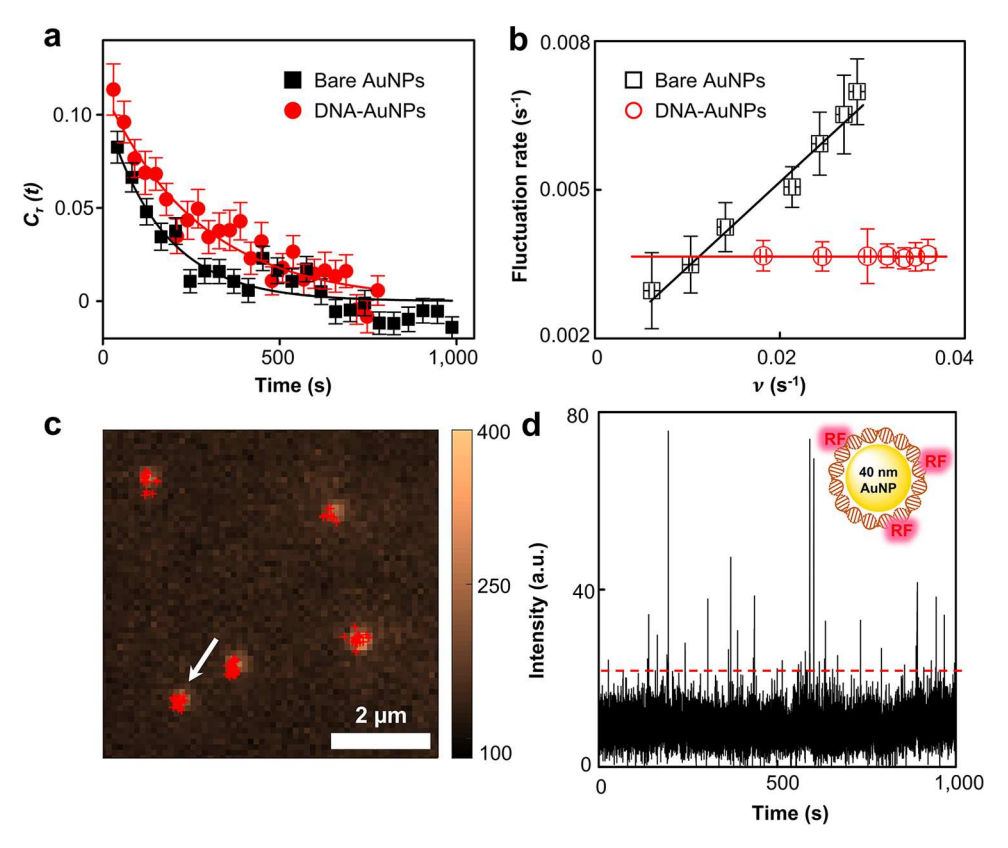


Figure 3. Oxidation reaction occurs in the DNA corona phase. (a) Autocorrelation function  $C_{\tau}(t)$  of the microscopic reaction time  $\tau$  from a single AuNP@DNA catalyzing the oxidation of 800 nM AR. The *x*-axis is a conversion from the turnover index to reaction time using the average turnover time of each nanozyme and averaged over >80 nanozymes. Solid curves are single exponential fits with decay constants of  $163 \pm 25$  and  $269 \pm 22$  s for the 5 nm AuNP and AuNP@DNA, respectively. (b) Dependence of the reactivity fluctuation rates on the turnover rates of the 5 nm AuNP and AuNP@DNA in AR oxidation. The *y*-axis is the inverse of the reactivity fluctuation correlation time obtained from  $C_{\tau}(t)$ . Solid lines are linear fits reflecting the adsorbate—surface interactions. (c) AR (400 nM) oxidation by a 40 nm AuNP@DNA. The 40 nm AuNPs are visible because of their photoluminescence signals. Red crosses are the centroids of generated RFs by fitting their emission signals with two-dimensional Gaussian functions. (d) Intensity versus time trajectory for the single 40 nm AuNP@DNA marked by the arrow in panel (c). Fluorescence intensity is integrated after subtracting the background emission signal from the 40 nm AuNP.

# Long-Range Oxidation of AR within the DNA Corona.

It is worth noting that the reactivity in a single AuNP@DNA fluctuates over time instead of being steady (Supporting Information Section S8). The fluctuating reactivity for a single nanozyme is known as "dynamic disorders", 36-39 a process hidden from conventional measurements. Interestingly, such fluctuations are not random. A catalytic "memory effect" seen as the autocorrelation decays for the waiting time  $\tau$  series reflects the underlying surface restructuring of the nanoparticle during catalysis<sup>35,36</sup> (Figure 3a). The product of the decay constant and average turnover time provides the correlation time for the nanozymes, which is related to the time scale for the surface restructuring. This correlation time is dependent on the reaction turnover for the 5 nm AuNP because of the adsorbate-surface interactions: 40 high substrate concentration simultaneously results in rapid reaction turnover and faster surface restructuring; hence, a linear dependence is seen (Figure 3b, black). Strikingly, the turnover rate-dependent surface restructuring no longer exists for the AuNP@DNA (Figure 3b, red). The lack of turnover rate dependence indicates that the adsorbate-surface interactions do not exist in the AuNP@DNA. This constant reactivity fluctuation seen in the AuNP@DNA is likely due to the conformational dynamics of the surrounding DNA since the fluctuation rate

matches with the previously reported values for the conformational changes.  $^{41,42}$ 

Based on the constant fluctuation rate and the decreased  $K_{\rm M}$ for the AuNP@DNA, we proposed a long-range reaction mechanism that occurs within the DNA corona (Supporting Information Section S7.3). The oxidation of AR starts with a reversible homolytic O-O bond cleavage of H<sub>2</sub>O<sub>2</sub> on AuNPs to generate OH radicals. These radicals oxidize the DNA bases at their proximity, converting them into radical cations. Subsequent charge (hole) transfer steps occur after the initial base oxidation 43-46 until the charge reaches the DNA-bound AR. Lastly, AR converts to RF through two consecutive oneelectron transfer processes, reducing the DNA base to its original state. To act as an effective catalyst, the AuNP serves as the radical initiation center, while the DNA corona functions as a radical transporter and a substrate binder that can be distally located away from the AuNP core. Compared to a natural enzyme such as HRP, the AuNP mimics the ferric center, while the DNA corona mimics the surrounding peptide. Unlike HRP, where only one ferric center and one reactive site exist, the nanocore provides multiple sites to generate OH radicals, whereas the charge transfer within the DNA corona converts multiple remote bases into reactive centers. Therefore, the DNA and AuNP synergistically contribute to the enhanced reactivity of the AuNP@DNA coronazyme.

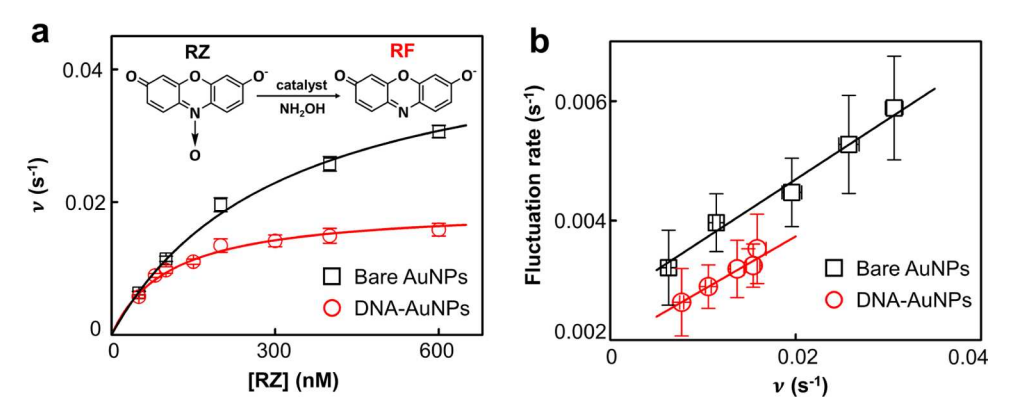


Figure 4. DNA corona phase does not participate in the dehydrogenase-mimicking reaction. (a) Dependence of the single-catalyst turnover rate  $\nu$ on [RZ] for the nanozyme-catalyzed reaction in a 50 mM pH 7.4 sodium phosphate buffer at 25 °C. A total of 195 bare AuNPs and 167 DNA@ AuNPs were measured; [NH<sub>2</sub>OH] = 1 mM. Inset: chemical equation of the N-deoxygenation RZ reduction. (b) Dependence of the reactivity fluctuation rates on the turnover rates of the 5 nm AuNP and AuNP@DNA in RZ reduction.

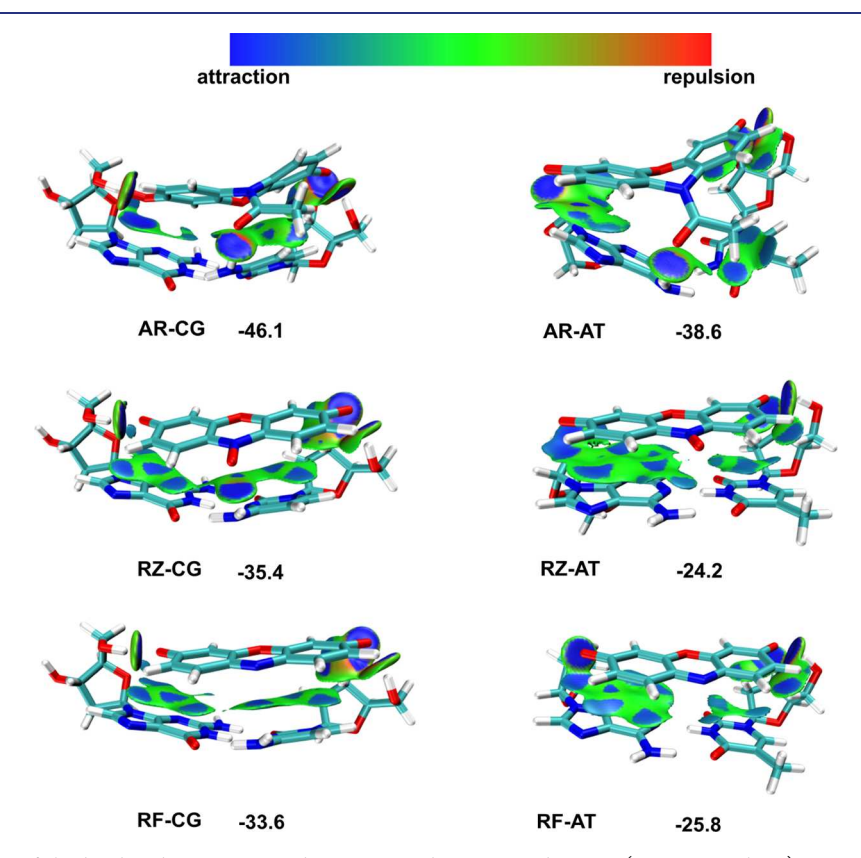


Figure 5. DFT calculation of the binding between DNA base pairs and reaction substrates (AR, RZ, and RF). Optimized structure and IGMH (independent gradient model based on Hirshfeld partition) map for AR-CG, AR-AT, RZ-CG, RZ-AT, RF-CG, and RF-AT. The values shown are binding energies in kcal/mol.

Another direct evidence supporting the long-range catalysis within the AuNP@DNA is the fluorescence quenching on a 40 nm AuNP. The 40 nm AuNP also has peroxidase reactivity by catalyzing the AR oxidation. Although its reactivity is apparent at the ensemble level, no fluorescence spot is seen at the singlemolecule level because fluorophore RFs are quenched at the AuNP surface<sup>47–49</sup> (Supporting Information Section S9). Surrounding the 40 nm AuNP with the DNA corona, however, restores the fluorescence emission of RFs (Figure 3c,d), suggesting that the RF formation occurs within the DNA corona rather than on the AuNP surface. The residence times of RF on the 5 nm AuNP@DNA and 40 nm AuNP@DNA are nearly the same (Figure S14), further supporting the direct

formation of RF within the DNA corona as it is known that RF desorption from the Au surface is dependent on the size of nanoparticles.<sup>50</sup> Previously, to facilitate sensing or chemical catalysis, complicated procedures have been designed to avoid the fluorescence quenching on larger AuNP without much success. 51-54 The use of DNA corona provides a facile approach to achieve this function.

Selectivity Enhancement within the DNA Corona. The fact that AuNPs can catalyze various enzymatic reactions indicates that a pristine AuNP lacks substrate specificity because different substrate molecules can adsorb and be activated on a AuNP surface. To determine the impact of the DNA corona on reaction specificity, we performed a

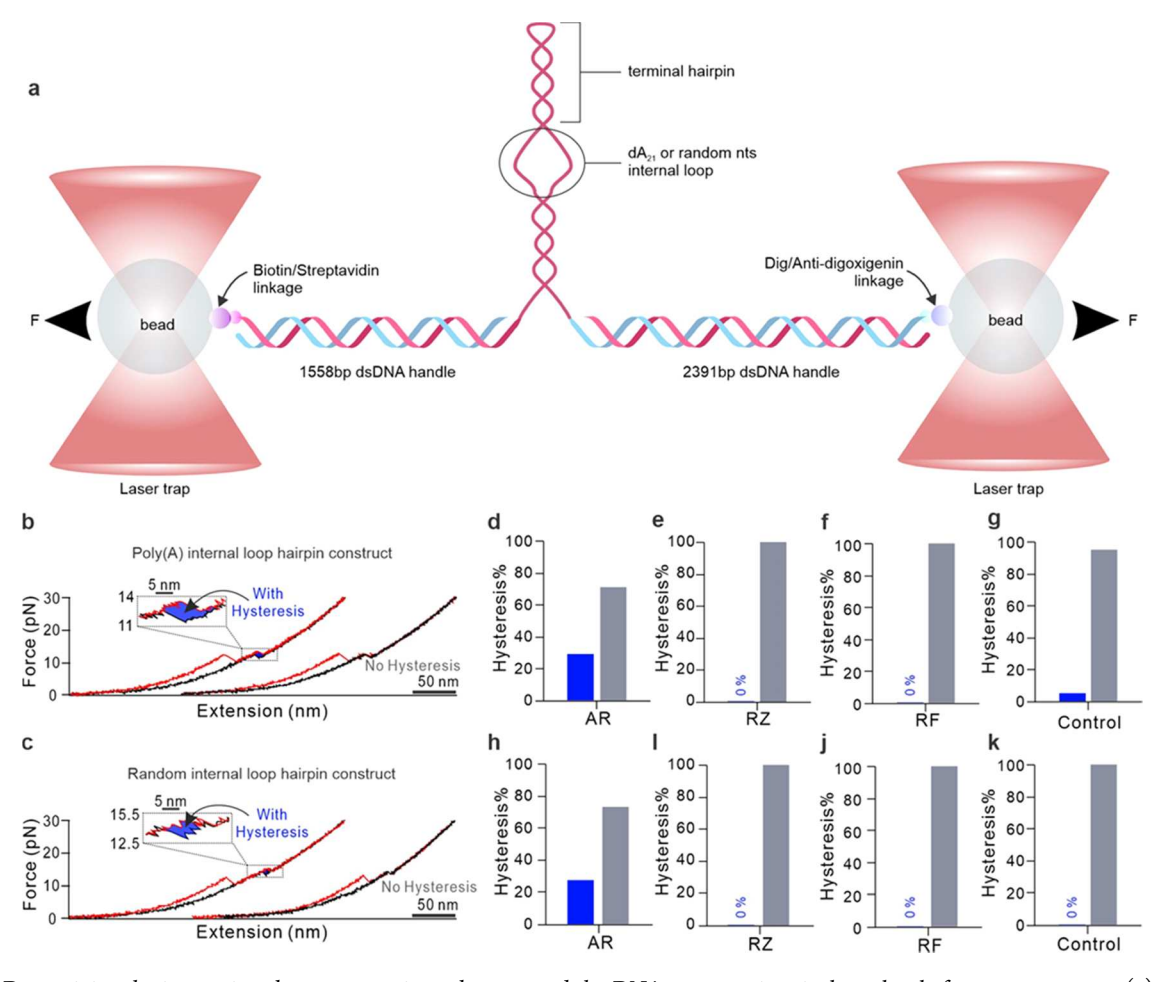


Figure 6. Determining the interactions between reaction substrates and the DNA corona using single-molecule force spectroscopy. (a) Schematic of an optical-tweezer setup. The corona DNA connects to two DNA handles, which are tethered by 1064 nm laser-trapped beads through the biotin/streptavidin links (see the Supporting Information and ref 23 for details). (b, c) Examples of FX curves for the AR and DNA hairpin interactions. DNA unfolds as the tensile force accumulates (red traces) and refolds after the force is reduced (black traces). A hysteresis may exist as the DNA-bound substrate delays the refolding (see blowup insets). Percentages of molecules that show hysteresis in FX curves for various substrates interacting with the DNA construct with (d-g) poly(A) and (h-k) random sequences in internal loops. A total of 17 DNAs were measured. Control means no substrate.

dehydrogenase-mimicking reaction in comparison to the AR oxidation. RZ, a nonfluorescent phenoxazine dye, is catalytically converted to the same RF in the presence of nanozymes and NH<sub>2</sub>OH<sup>35,55</sup> (Figure 4a inset). Using the same singlemolecule microscopy, we found that the [RZ]-dependent reactivity also followed the Michaelis-Menten kinetics in a 50 mM sodium phosphate buffer (pH 7.4).  $k_{cat}n$  and  $K_{M}$  for the 5 nm AuNP are 0.047  $\pm$  0.002 s<sup>-1</sup> and 0.31  $\pm$  0.02  $\mu$ M, respectively, giving a catalytic efficiency ( $k_{\rm cat}n/K_{\rm M}$ ) at 0.15  $\pm$  $0.01 \text{ s}^{-1} \mu\text{M}^{-1}$ . As a nanozyme, the 5 nm pristine AuNP exhibits almost identical catalytic efficiency in RZ reduction and AR oxidation, thus lacking specificity. After adding the DNA corona to the AuNP, the  $k_{\rm cat}n$  and  $K_{\rm M}$  become 0.019  $\pm$  $0.001~{\rm s}^{-1}$  and  $0.10~\pm~0.01~\mu{\rm M}$ , respectively, giving a catalytic efficiency at  $0.18 \pm 0.02 \text{ s}^{-1} \mu\text{M}^{-1}$ . Unlike the AR oxidation, no catalytic efficiency enhancement is seen, suggesting that the DNA corona does not favor the RZ reduction.

Notably, the reactivity fluctuation analyses show a clear dependence on the turnover rate during the RZ reduction (Figure 4b). The surface restructuring rate for both the 5 nm AuNP and AuNP@DNA increases linearly with an increasing turnover rate. This result strongly suggests that the RZ reduction only occurs on the AuNP surface. Since the DNA

corona does not directly participate in the reaction, its presence blocks the available surface sites on the AuNP, leading to decreased reactivity. Likewise, the lower surface restructuring rate across the concentration range is due to the surface passivation by the adsorbed DNA corona (Supporting Information Section S7.4).

Origin of Reactivity and Selectivity Enhancement within the DNA Corona. To investigate the interaction mechanism between the DNA corona and substrate molecules, we performed DFT calculations at the B3LYP-D3BJ level (Supporting Information Section S10). Electrostatic potential (ESP) calculation indicates that AR and RZ may interact with all four bases (Supporting Information Figure S15). The binding energies for AR on base pairs A-T, C-G, and the gold binding bases A-A are -38.6, -46.1, and -31.0 kcal/ mol, respectively (Figures 5, S17, and S18), suggesting that AR tends to strongly adsorb on the DNA corona. DFT calculation indicates that the A-T base pair adopts a planar structure under normal conditions. However, its planarity would undergo a topographic change after AR binding (Supporting Information Figure S19). The significant binding affinities of AR to DNA bases justify our single-molecule observation in which the 5 nm Au surface becomes less preferred by the AR

molecules during catalysis. As a comparison, the RZ-DNA corona interactions are substantial but noticeably weaker than AR-DNA. The binding energies on base pairs A-T, C-G, and A-A are -24.2, -35.4, and -17.7 kcal/mol, respectively (Figures 5, S17, and S18). The relatively lower binding energies for RZ justify the enhanced reaction selectivity of AR over RZ: the DNA corona is more favorable toward the AR adsorption, and the reaction occurs directly on DNA bases. Hence, stronger binding is favorable for enriching the reactant AR around reactive sites, resulting in enhanced oxidation efficiency. On the contrary, the DNA corona acts as a physical filter for RZ reduction, preventing the RZ substrate from accessing the reactive sites. The product RF has binding energies on base pairs A-T, C-G, and A-A at -25.8, -33.6, and -21.2 kcal/mol, respectively. Therefore, a significant binding energy loss exists for the AR  $\rightarrow$  RF oxidation: the lossof-affinity principle facilitates the product displacement. 56 No significant binding energy change exists for the RZ reduction to RF. Thus, the catalytic efficiency for the RZ reduction remains the same in the presence of the DNA corona.

To confirm these substrate-DNA corona interactions, we carried out single-molecule force spectroscopy using a dualtrap optical-tweezer setup (Figure 6a).<sup>57</sup> The DNA structure unfolds when force is increased (Figure 6b,c, red), while it refolds after the force is released (Figure 6b,c, black), giving a reversible force-extension (FX) curve. The sudden change in FX curves marks the unfolding of the DNA structure. Among the 17 tested DNAs, 29% feature an apparent hysteresis after the AR adsorption (Figure 6d). In comparison, without any ligand (control, Figure 6g), hysteresis is insignificant (5%). This hysteresis suggests that AR can bind to the DNA structure, which delays the refolding of DNA. In another comparison, neither RZ nor RF features the same hysteresis (Figure 6e,f), suggesting that their binding affinities to DNAs are weaker. To probe the location of the AR binding, we randomized AuNP-binding single-stranded poly(adenosine) to scrambled sequences, CAACATATCAACCTCAAGGAG and GAATCACTCTAACTATACAAC. Hysteresis was again observed only for AR (Figure 6c,h-k), suggesting that the binding occurs at the duplex region of the DNA structure (Figure 6a). These results aligned well with the DFT calculation (Figure 5), which showed preferential binding of the AR to DNA base pairs instead of unpaired bases.

### CONCLUSIONS

Based on the experimental and simulation results, we discover that the AuNP@DNA demonstrates much increased catalytic efficiency and substrate specificity relative to pristine AuNPs. Its efficiency (0.75 s<sup>-1</sup>  $\mu M^{-1}$ ) is also higher than natural HRP enzymes (average  $0.28 \text{ s}^{-1} \mu\text{M}^{-1}$ ), most DNAzymes (averaged at  $0.63 \text{ s}^{-1} \mu\text{M}^{-1}$ ), and >10 times higher than nanozymes (averaged at 0.06 s<sup>-1</sup>  $\mu$ M<sup>-1</sup>, Supporting Information Table S3) catalyzing the AR  $\rightarrow$  RF reaction. The pivotal component in the AuNP@DNA composite is the DNA corona, which serves as the scaffold for catalytic transformation. A DNA corona selectively filters substrates in the reaction mixture, offering high binding affinities to desired molecules. Individual bases on the DNA serve as reactive sites after the substrate binding, while the DNA strand serves as the media to transport radicals/charges generated remotely on the surface of a nanocore. Moreover, the DNA corona features binding energy loss after product formation, accelerating the reaction turnovers. Such orchestrated structure and synergistic function

closely mimic those of enzymes; therefore, we name this new device a "coronazyme". Unlike previous redox catalysis (enzyme/nanozyme/DNAzyme) in which a cascade of redox pairs is closely coupled at the reaction site, coronazyme decouples the cascade by a long-range hole/charge transfer in the corona phase. The separate locations relieve the requirement for a single reaction site with multiple functionalities. This, therefore, facilitates modular evolvement of better catalysts by adopting the best material for each function instead of using a single material with multiple but subpar properties. We envision that optimizing the morphology of the nanoparticle core and the structure of the DNA corona will further improve the performances of coronazymes.

#### ASSOCIATED CONTENT

# **s** Supporting Information

The Supporting Information is available free of charge at https://pubs.acs.org/doi/10.1021/jacs.2c12367.

Detailed procedure of coronazyme synthesis; fluorogenic probing reactions; optical-tweezer setup for force spectroscopy; single-molecule fluorescence detection; single-molecule kinetic analyses; reactivity fluctuation; reactivity of the 40 nm AuNP@DNA; computational studies and the corresponding references (PDF)

#### AUTHOR INFORMATION

### **Corresponding Authors**

Hanbin Mao – Department of Chemistry and Biochemistry, Kent State University, Kent, Ohio 44242, United States; orcid.org/0000-0002-6720-9429; Email: hmao@kent.edu

Hao Shen — Department of Chemistry and Biochemistry, Kent State University, Kent, Ohio 44242, United States; orcid.org/0000-0002-2798-5861; Email: hshen7@kent.edu

#### **Authors**

Li Zuo – Department of Chemistry and Biochemistry, Kent State University, Kent, Ohio 44242, United States; School of Chemistry and Chemical Engineering, Nanjing University, Nanjing 210008 Jiangsu, China

Kehao Ren – Department of Chemistry and Biochemistry, Kent State University, Kent, Ohio 44242, United States

Xianming Guo – School of Chemistry and Chemical Engineering, Nanjing University, Nanjing 210008 Jiangsu, China

Pravin Pokhrel – Department of Chemistry and Biochemistry, Kent State University, Kent, Ohio 44242, United States; orcid.org/0000-0003-4259-6087

Bishal Pokhrel – Department of Chemistry and Biochemistry, Kent State University, Kent, Ohio 44242, United States

Mohammad Akter Hossain – Department of Chemistry and Biochemistry, Kent State University, Kent, Ohio 44242, United States

Zhao-Xu Chen – School of Chemistry and Chemical Engineering, Nanjing University, Nanjing 210008 Jiangsu, China; orcid.org/0000-0002-5444-776X

Complete contact information is available at: https://pubs.acs.org/10.1021/jacs.2c12367

#### Notes

The authors declare no competing financial interest.

#### ACKNOWLEDGMENTS

The authors thank the Kent State University for financial support. H.M. acknowledges the National Science Foundation (NSF) (No. CBET1904921) and National Institute of Health (NIH) (No. R01 CA236350) for grant support. Z.-X.C. acknowledges the National Natural Science Foundation of China (No. 22072064) for grant support.

#### REFERENCES

- (1) Fan, K.; Xi, J.; Fan, L.; Wang, P.; Zhu, C.; Tang, Y.; Xu, X.; Liang, M.; Jiang, B.; Yan, X.; Gao, L. In vivo guiding nitrogen-doped carbon nanozyme for tumor catalytic therapy. *Nat. Commun.* **2018**, *9*, No. 1440.
- (2) Ji, S.; Jiang, B.; Hao, H.; Chen, Y.; Dong, J.; Mao, Y.; Zhang, Z.; Gao, R.; Chen, W.; Zhang, R.; Liang, Q.; Li, H.; Liu, S.; Wang, Y.; Zhang, Q.; Gu, L.; Duan, D.; Liang, M.; Wang, D.; Yan, X.; Li, Y. Matching the kinetics of natural enzymes with a single-atom iron nanozyme. *Nat. Catal.* **2021**, *4*, 407–417.
- (3) Wu, J.; Wang, X.; Wang, Q.; Lou, Z.; Li, S.; Zhu, Y.; Qin, L.; Wei, H. Nanomaterials with enzyme-like characteristics (nanozymes): next-generation artificial enzymes (II). *Chem. Soc. Rev.* **2019**, *48*, 1004–1076.
- (4) Huang, Y.; Ren, J.; Qu, X. Nanozymes: Classification, Catalytic Mechanisms, Activity Regulation, and Applications. *Chem. Rev.* **2019**, *119*, 4357–4412.
- (5) Liang, M.; Yan, X. Nanozymes: from new concepts, mechanisms, and standards to applications. Acc. Chem. Res. 2019, 52, 2190–2200.
- (6) Borggräfe, J.; Victor, J.; Rosenbach, H.; Viegas, A.; Gertzen, C. G. W.; Wuebben, C.; Kovacs, H.; Gopalswamy, M.; Riesner, D.; Steger, G.; Schiemann, O.; Gohlke, H.; Span, I.; Etzkorn, M. Timeresolved structural analysis of an RNA-cleaving DNA catalyst. *Nature* 2022, 601, 144–149.
- (7) Hollenstein, M.; Hipolito, C.; Lam, C.; Dietrich, D.; Perrin, D. M. A Highly Selective DNAzyme Sensor for Mercuric Ions. *Angew. Chem.* **2008**, *120*, 4307.
- (8) Li, W.; Li, Y.; Liu, Z.; Lin, B.; Yi, H.; Xu, F.; Nie, Z.; Yao, S. Insight into G-quadruplex-hemin DNAzyme/RNAzyme: adjacent adenine as the intramolecular species for remarkable enhancement of enzymatic activity. *Nucleic Acids Res.* **2016**, *44*, 7373–7384.
- (9) Tang, J.; Hou, L.; Tang, D.; Zhang, B.; Zhou, J.; Chen, G. Hemin/G-quadruplex-based DNAzyme concatamers as electrocatalysts and biolabels for amplified electrochemical immunosensing of IgG1. Chem. Commun. 2012, 48, 8180–8182.
- (10) Travascio, P.; Li, Y.; Sen, D. DNA-enhanced peroxidase activity of a DNA aptamer-hemin complex. *Chem. Biol.* **1998**, *5*, 505–517.
- (11) Sun, D.; Lin, X.; Lu, J.; Wei, P.; Luo, Z.; Lu, X.; Chen, Z.; Zhang, L. DNA nanotetrahedron-assisted electrochemical aptasensor for cardiac troponin I detection based on the co-catalysis of hybrid nanozyme, natural enzyme and artificial DNAzyme. *Biosens. Bioelectron.* **2019**, *142*, No. 111578.
- (12) Zhang, L.; Chu, M.; Ji, C.; Tan, J.; Yuan, Q. Preparation, applications, and challenges of functional DNA nanomaterials *Nano Res.* 2022, DOI: 10.1007/s12274-022-4793-5.
- (13) Zhu, X.; Mao, X.; Wang, Z.; Feng, C.; Chen, G.; Li, G. Fabrication of nanozyme@DNA hydrogel and its application in biomedical analysis. *Nano Res.* **2017**, *10*, 959–970.
- (14) Zeng, C.; Lu, N.; Wen, Y.; Liu, G.; Zhang, R.; Zhang, J.; Wang, F.; Liu, X.; Li, Q.; Tang, Z.; Zhang, M. Engineering Nanozymes Using DNA for Catalytic Regulation. *ACS Appl. Mater. Interfaces* **2019**, *11*, 1790–1799.
- (15) Chen, X.; Wang, Y.; Dai, X.; Ding, L.; Chen, J.; Yao, G.; Liu, X.; Luo, S.; Shi, J.; Wang, L.; Nechushtai, R.; Pikarsky, E.; Willner, I.; Fan, C.; Li, J. Single-Stranded DNA-Encoded Gold Nanoparticle Clusters as Programmable Enzyme Equivalents. *J. Am. Chem. Soc.* **2022**, *144*, 6311–6320.
- (16) Mirkin, C. A.; Letsinger, R. L.; Mucic, R. C.; Storhoff, J. J. A DNA-based method for rationally assembling nanoparticles into macroscopic materials. *Nature* **1996**, 382, 607–609.

- (17) Nel, A. E.; Mädler, L.; Velegol, D.; Xia, T.; Hoek, E. M. V.; Somasundaran, P.; Klaessig, F.; Castranova, V.; Thompson, M. Understanding biophysicochemical interactions at the nano-bio interface. *Nat. Mater.* **2009**, *8*, 543–557.
- (18) Ohta, S.; Glancy, D.; Chan, W. C. W. DNA-controlled dynamic colloidal nanoparticle systems for mediating cellular interaction. *Science* **2016**, *351*, 841–845.
- (19) Tan, L. H.; Xing, H.; Lu, Y. DNA as a Powerful Tool for Morphology Control, Spatial Positioning, and Dynamic Assembly of Nanoparticles. *Acc. Chem. Res.* **2014**, *47*, 1881–1890.
- (20) Yang, F.; Zuo, X.; Fan, C.; Zhang, X.-E. Biomacromolecular nanostructures-based interfacial engineering: from precise assembly to precision biosensing. *Natl. Sci. Rev.* **2018**, *5*, 740–755.
- (21) Perrin, D. M.; Garestier, T.; Hélène, C. Bridging the Gap between Proteins and Nucleic Acids: A Metal-Independent RNAseA Mimic with Two Protein-Like Functionalities. *J. Am. Chem. Soc.* **2001**, 123, 1556–1563.
- (22) Landry, M. P.; Vuković, L.; Kruss, S.; Bisker, G.; Landry, A. M.; Islam, S.; Jain, R.; Schulten, K.; Strano, M. S. Comparative Dynamics and Sequence Dependence of DNA and RNA Binding to Single Walled Carbon Nanotubes. *J. Phys. Chem. C* **2015**, *119*, 10048–10058.
- (23) Pokhrel, P. R.; Ren, K.; Shen, H.; Mao, H. Mechanical Stability of DNA Corona Phase on Gold Nanospheres. *Langmuir* **2022**, *38*, 13569–13576.
- (24) Bisker, G.; Dong, J.; Park, H. D.; Iverson, N. M.; Ahn, J.; Nelson, J. T.; Landry, M. P.; Kruss, S.; Strano, M. S. Protein-targeted corona phase molecular recognition. *Nat. Commun.* **2016**, *7*, No. 10241.
- (25) Park, M.; Salem, D. P.; Parviz, D.; Gong, X.; Silmore, K. S.; Lew, T. T. S.; Khong, D. T.; Ang, M. C.-Y.; Kwak, S.-Y.; Chan-Park, M. B.; Strano, M. S. Measuring the Accessible Surface Area within the Nanoparticle Corona Using Molecular Probe Adsorption. *Nano Lett.* **2019**, *19*, 7712–7724.
- (26) Zheng, X.; Liu, Q.; Jing, C.; Li, Y.; Li, D.; Luo, W.; Wen, Y.; He, Y.; Huang, Q.; Long, Y. T.; Fan, C. Catalytic gold nanoparticles for nanoplasmonic detection of DNA hybridization. *Angew. Chem.* **2011**, 123, 12200–12204.
- (27) Park, K. S.; Kim, M. I.; Cho, D. Y.; Park, H. G. Label-free colorimetric detection of nucleic acids based on target-induced shielding against the peroxidase-mimicking activity of magnetic nanoparticles. *Small* **2011**, *7*, 1521–1525.
- (28) Hizir, M. S.; Top, M.; Balcioglu, M.; Rana, M.; Robertson, N. M.; Shen, F.; Sheng, J.; Yigit, M. V. Multiplexed activity of perAuxidase: DNA-capped AuNPs act as adjustable peroxidase. *Anal. Chem.* **2016**, *88*, 600–605.
- (29) Liu, B.; Liu, J. Accelerating peroxidase mimicking nanozymes using DNA. *Nanoscale* **2015**, 7, 13831–13835.
- (30) Sauer, M.; Hofkens, J.; Enderlein, J. Handbook of Fluorescence Spectroscopy and Imaging: From Ensemble to Single Molecules; John Wiley & Sons, 2010; ISBN 978-3-527-31669-4.
- (31) Huang, B.; Wang, W.; Bates, M.; Zhuang, X. Three-Dimensional Super-Resolution Imaging by Stochastic Optical Reconstruction Microscopy. *Science* **2008**, *319*, 810–813.
- (32) Ovesný, M.; Křížek, P.; Borkovec, J.; Švindrych, Z.; Hagen, G. M. ThunderSTORM: a comprehensive ImageJ plug-in for PALM and STORM data analysis and super-resolution imaging. *Bioinformatics* **2014**, *30*, 2389–2390.
- (33) Mao, H.; Luchette, P. An integrated laser-tweezers instrument for microanalysis of individual protein aggregates. *Sens. Actuators, B* **2008**, *129*, 764–771.
- (34) Gorris, H. H.; Walt, D. R. Mechanistic Aspects of Horseradish Peroxidase Elucidated through Single-Molecule Studies. *J. Am. Chem. Soc.* **2009**, *131*, 6277–6282.
- (35) Xu, W.; Kong, J. S.; Yeh, Y.-T. E.; Chen, P. Single-molecule nanocatalysis reveals heterogeneous reaction pathways and catalytic dynamics. *Nat. Mater.* **2008**, *7*, 992–996.
- (36) Lu, H. P.; Xun, L.; Xie, X. S. Single-Molecule Enzymatic Dynamics. *Science* **1998**, 282, 1877–1882.

- (37) Min, W.; English, B. P.; Luo, G.; Cherayil, B. J.; Kou, S. C.; Xie, X. S. Fluctuating Enzymes: Lessons from Single-Molecule Studies. *Acc. Chem. Res.* **2005**, *38*, 923–931.
- (38) Ye, R.; Mao, X.; Sun, X.; Chen, P. Analogy between Enzyme and Nanoparticle Catalysis: A Single-Molecule Perspective. *ACS Catal.* **2019**, *9*, 1985–1992.
- (39) Roeffaers, M. B. J.; De Cremer, G.; Uji-i, H.; Muls, B.; Sels, B. F.; Jacobs, P. A.; De Schryver, F. C.; De Vos, D. E.; Hofkens, J. Single-molecule fluorescence spectroscopy in (bio)catalysis. *Proc. Natl. Acad. Sci.* **2007**, *104*, 12603–12609.
- (40) Imbihl, R.; Ertl, G. Oscillatory kinetics in heterogeneous catalysis. *Chem. Rev.* **1995**, *95*, *697*–733.
- (41) Long, X.; Parks, J. W.; Bagshaw, C. R.; Stone, M. D. Mechanical unfolding of human telomere G-quadruplex DNA probed by integrated fluorescence and magnetic tweezers spectroscopy. *Nucleic Acids Res.* **2013**, *41*, 2746–2755.
- (42) Lee, M.; Kim, S. H.; Hong, S.-C. Minute negative superhelicity is sufficient to induce the B-Z transition in the presence of low tension. *Proc. Natl. Acad. Sci.* **2010**, *107*, 4985–4990.
- (43) Genereux, J. C.; Barton, J. K. Mechanisms for DNA Charge Transport. *Chem. Rev.* **2010**, *110*, 1642–1662.
- (44) O'Neil, M. A.; Barton, J. K. DNA Charge Transport: Conformationally Gated Hopping through Stacked Domains. J. Am. Chem. Soc. 2004, 126, 11471–11483.
- (45) Renaud, N.; Berlin, Y. A.; Lewis, F. D.; Ratner, M. A. Between Superexchange and Hopping: An Intermediate Charge-Transfer Mechanism in Poly(A)-Poly(T) DNA Hairpins. *J. Am. Chem. Soc.* **2013**, *135*, 3953–3963.
- (46) Ratner, M. Electronic motion in DNA. *Nature* **1999**, 397, 480–481.
- (47) Cannone, F.; Chirico, G.; Bizzarri, A. R.; Cannistraro, S. Quenching and Blinking of Fluorescence of a Single Dye Molecule Bound to Gold Nanoparticles. *J. Phys. Chem. B* **2006**, *110*, 16491–16498
- (48) Dulkeith, E.; Morteani, A. C.; Niedereichholz, T.; Klar, T. A.; Feldmann, J.; Levi, S. A.; van Veggel, F. C. J. M.; Reinhoudt, D. N.; Möller, M.; Gittins, D. I. Fluorescence Quenching of Dye Molecules near Gold Nanoparticles: Radiative and Nonradiative Effects. *Phys. Rev. Lett.* **2002**, *89*, No. 203002.
- (49) Dulkeith, E.; Ringler, M.; Klar, T. A.; Feldmann, J.; Muñoz Javier, A.; Parak, W. J. Gold Nanoparticles Quench Fluorescence by Phase Induced Radiative Rate Suppression. *Nano Lett.* **2005**, *5*, 585–589.
- (50) Zhou, X.; Xu, W.; Liu, G.; Panda, D.; Chen, P. Size-Dependent Catalytic Activity and Dynamics of Gold Nanoparticles at the Single-Molecule Level. *J. Am. Chem. Soc.* **2010**, *132*, 138–146.
- (51) Abadeer, N. S.; Brennan, M. R.; Wilson, W. L.; Murphy, C. J. Distance and Plasmon Wavelength Dependent Fluorescence of Molecules Bound to Silica-Coated Gold Nanorods. *ACS Nano* **2014**, *8*, 8392–8406.
- (52) Schneider, G.; Decher, G.; Nerambourg, N.; Praho, R.; Werts, M. H. V.; Blanchard-Desce, M. Distance-Dependent Fluorescence Quenching on Gold Nanoparticles Ensheathed with Layer-by-Layer Assembled Polyelectrolytes. *Nano Lett.* **2006**, *6*, 530–536.
- (53) Zhou, X.; Andoy, N. M.; Liu, G.; Choudhary, E.; Han, K.-S.; Shen, H.; Chen, P. Quantitative super-resolution imaging uncovers reactivity patterns on single nanocatalysts. *Nat. Nanotechnol.* **2012**, *7*, 237–241.
- (54) Andoy, N. M.; Zhou, X.; Choudhary, E.; Shen, H.; Liu, G.; Chen, P. Single-Molecule Catalysis Mapping Quantifies Site-Specific Activity and Uncovers Radial Activity Gradient on Single 2D Nanocrystals. *J. Am. Chem. Soc.* **2013**, *135*, 1845–1852.
- (55) Nigra, M. M.; Arslan, I.; Katz, A. Gold nanoparticle-catalyzed reduction in a model system: Quantitative determination of reactive heterogeneity of a supported nanoparticle surface. *J. Catal.* **2012**, 295, 115–121.
- (56) Gluhacevic von Krüchten, D.; Roth, M.; Seitz, O. DNA-Templated Reactions with High Catalytic Efficiency Achieved by a Loss-of-Affinity Principle. *J. Am. Chem. Soc.* **2022**, *144*, 10700–10704.

(57) Koirala, D.; Dhakal, S.; Ashbridge, B.; Sannohe, Y.; Rodriguez, R.; Sugiyama, H.; Balasubramanian, S.; Mao, H. A single-molecule platform for investigation of interactions between G-quadruplexes and small-molecule ligands. *Nat. Chem.* **2011**, *3*, 782–7.

# **□** Recommended by ACS

# Spherical Nucleic Acid Probe Based on 2'-Fluorinated DNA Functionalization for High-Fidelity Intracellular Sensing

Tao Zeng, Huanghao Yang, et al.

DECEMBER 15, 2022

ANALYTICAL CHEMISTRY

READ 🗹

# Switchable DNA Photocatalysts for Radical Polymerization Controlled by Chemical Stimuli

Caleb A. Cox, Jeffrey D. Martell, et al.

JANUARY 11, 2023

JOURNAL OF THE AMERICAN CHEMICAL SOCIETY

READ 🗹

# Non-Invasive, Reliable, and Fast Quantification of DNA Loading on Gold Nanoparticles by a One-Step Optical Measurement

Jaewon Lee and Seungwoo Lee

JANUARY 12, 2023

ANALYTICAL CHEMISTRY

READ 🗹

# Self-Stacking Autocatalytic Molecular Circuit with Minimal Catalytic DNA Assembly

Ruomeng Li, Fuan Wang, et al.

JANUARY 26, 2023

JOURNAL OF THE AMERICAN CHEMICAL SOCIETY

READ 🗹

Get More Suggestions >